TERAHERTZ SHAPIRO STEPS IN HIGH TEMPERATURE SNS JOSEPHSON JUNCTIONS*

P. A. Rosenthal and E. N. Grossman

Electromagnetic Technology Division
National Institute of Standards and Technology
325 Broadway
Boulder, CO 80303

Abstract

We have studied the far infrared behavior of high-T_C superconductor-normal metal-superconductor (SNS) microbridges with properties well suited for sub-THz and THz applications. We have fabricated YBCO junctions with $T_C > 85$ K and critical current-resistance products (I_CR_N) as high as 10 mV at 4.2 K. These are the highest I_CR_N products reported to date for micrfabricated Josephson junctions of any material. The junctions were integrated at the feeds of planar log-periodic antennas made from noble metal thin films. The junctions had D.C. normal state resistances R_N between 10 and 40 Ω, well matched to the antenna's estimated R.F. impedance of 53 Ω. A far infrared laser was focused onto the antenna-coupled junctions through the backside of the substrate via a plano-convex polyethylene lens and a hemispherical silicon lens. Radiation at 404, 760, and 992 GHz induced pronounced Shapiro steps (i.e. constant voltage steps at voltages n(hv/2e), n= 0,1,2,...) in the current voltage characteristics as well as modulation of the critical current. The amplitude of the Shapiro steps rapidly decays at voltages above 1-1.5 I_CR_N corresponding to a maximum frequency cutoff of ~ 8 THz. These are the first far infrared measurements performed on high T_C junctions. Measurements of the power, frequency, and temperature dependence of the Shapiro steps are presented and discussed in the context of a resistively and capacitively shunted junction (RCSJ) model. A value of 4.5 fF for the capacitance is inferred from the hysteresis of the slightly underdamped current-voltage characteristics.

I. Introduction

The potential of Josephson junctions for various submillimeter and THz applications has been of interest for some time.[1] Furthermore, the discovery of high temperature superconductivity and subsequent advances in the art of fabrication of Josephson junctions and thin film structures has renewed interest in various high frequency applications of Josephson junctions which are not addressed by practical low T_c devices.[2] The frequency scale for all Josephson effects is set by the I_cR_N product through the definition of the dimensionless or reduced frequency $\Omega = h\nu/(2eI_cR_N)$, where ν is the real frequency, $h/2e$ is the flux quantum and I_c and R_N, the critical current and normal state resistance, enter in product form. The I_cR_N product or characteristic voltage is fundamentally limited by the superconducting energy gap.[3] When the junctions are strongly damped by additional shunt conductance, the characteristic voltage is substantially reduced. The most successful high T_c junction approaches to date, such as grain-boundary junctions (GBJs)[4,5], and step-edge superconductor/normal metal/superconductor (SNS) junctions[6,7] have achieved I_cR_N products of 1-2 mV, comparable to that achieved with Nb (for which the tunneling gap $2\Delta = 2.9$ mV at 4 K). However, an important distinction should be made : Nb tunnel junctions with the full gap-limited characteristic voltage are extremely underdamped whereas the high T_c junctions have generally been strongly overdamped, as most clearly evidenced by their non-hysteretic current voltage characteristics. It has been shown[8] that the strongly damped resistively shunted junction (RSJ) model describes well the power and frequency dependence of the Shapiro steps and critical currents in high Tc SNS junctions at reduced frequencies $\Omega = h\nu/(2eI_cR_N) < 1$ when the I_cR_N product is ≤ 0.5 mV. These facts suggest that high temperature superconducting Josephson junctions have the potential for much higher I_cR_N products, extending the range of useful Josephson effects to much higher frequencies.

We have recently developed a technique for fabricating low capacitance SNS junctions from $Y_1B_2Cu_3O_7$ (YBCO) with I_cR_N products as high as 10 mV, as measured from D.C. current voltage characteristics. The characteristic frequency associated with a 10 mV characteristic voltage is 4.8 THz. Our goal in this work was to determine to what extent the RSJ like behavior at low characteristic voltages and reduced frequencies persists to high characteristic voltages and high reduced and real frequencies. We believe that the high characteristic voltages and operating frequencies of these devices represent a breakthrough in THz device technology.

In this work, we investigate the high frequency behavior of selected junctions of this type using quasioptical coupling techniques and a far infrared laser. In section II of this paper we present an overview of our fabrication process for superconductor/normal metal/superconductor Josephson junctions with integrated THz bandwidth antennas. In section III we describe the optics and electronics used to perform far infrared measurements. In section IV we present the results of measurements of the power, frequency and temperature dependence of the current-voltage characteristics of selected Josephson junctions under irradiation by signals up to 1 THz. The measurements demonstrate quasioptical coupling of a far infrared laser into a high temperature superconductor (HTS) Josephson junction as evidenced by Shapiro steps induced in the junction current-voltage characteristics. We discuss the results of these measurements in the context of a resistively shunted junction model.

II. Fabrication

Junctions were fabricated by a variant of the process presented by Ono et al.[7] The processing sequence is shown in Fig. 1. First, roughly perpendicular steps approximately 100 nm deep were etched by ion milling into (100) $LaAlO_3$ substrates. It was found that, for $LaAlO_3$ substrates, 300 nm thick niobium etch masks patterned by photolithography and reactive ion etching yielded better step-edge profiles than did a simple photoresist etch mask. Because Nb etches more quickly than NbO_x we found that spraying a small amount of oxygen onto the substrates during the milling process helped to sharpen the steps and reduce the required Nb mask thickness. The substrates were rotated during the ion milling process, and a 1000 eV Ar ion beam at 1 mA/cm^2 cut the steps in approximately 10 minutes. After the steps were etched, the Nb masks were stripped off in a CF_4/O_2 plasma etch, and the samples were cleaned carefully. Next, a film of $Y_1Ba_2Cu_3O_7$ was grown on the substrate by laser deposition. The samples were held at approximately a 40° angle relative to the laser plume to cause the superconducting film to break across the step edge. The YBCO was deposited in 27 Pa (200 mT) of O_2 at a substrate temperature of 775 °C at a rate of 1.3 nm/sec, using a KrF excimer laser at 10 Hz with a measured beam energy of 120 mJ/pulse focused onto a 10 mm^2 area, for a fluence of 1.2 J/cm^2. Using our deposition parameters we routinely grow films with smooth morphologies, critical temperatures over 90 K, and critical current densities above 10^6 A/cm^2 at 77 K.[9] After the superconducting film is deposited the substrate heater is rotated to normal incidence, the deposition chamber is pumped down and a

normal metal (Au, Ag, or AuAg alloy) is deposited to a thickness of ~50 nm. The samples are then further rotated 30° and another 100 nm or so of normal metal are deposited. The normal metal films are grown by sputtering without exposing the sample to atmospheric pressure to minimize surface degradation and contact resistance at the SN interfaces, while the deposition angles help the normal metal make a robust bridge across the break in the superconductor at the step. After deposition, the samples are removed, and the SN bilayers are patterned into bridges typically 6 μm wide.

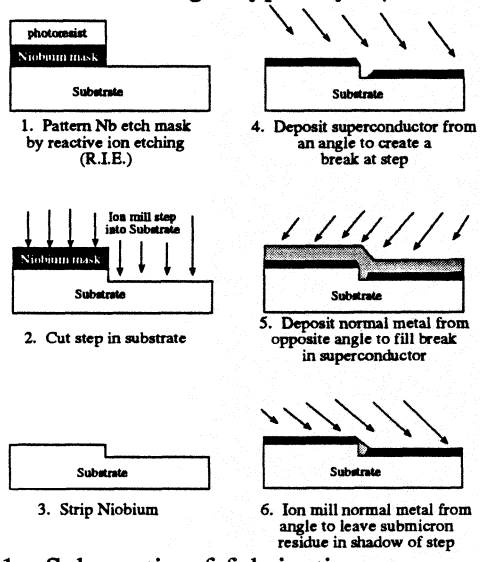

Fig. 1. Schematic of fabrication sequence to produce step-edge SNS Josephson junctions.

Antennas are fabricated by liftoff, with another deposition step consisting of a 5 nm layer of Ti for adhesion followed by a ~140 nm thick film of Ag. The antennas used in all of the far infrared measurements were of the log-periodic type[10] depicted in Fig. 2 (a) with a minimum tooth radius of ~12 μm at the feed and a maximum tooth radius of 2 mm. The bow angle was 45°, and the tooth and slot angles were each 45°. This design is self-complementary and self-similar, so to a good approximation the impedance should be purely real and almost frequency independent over a bandwidth of approximately .14 - 2.3 THz.[11] Using the quasistatic expression for the antenna impedance $Z_{ant} = Z_0 / \sqrt{[2(1+\varepsilon_r)]}$ we estimate an impedance of 53 Ω assuming a dielectric constant of 24 for the $LaAlO_3$ substrate. After the antenna liftoff, the samples were diced and tested at D.C. The best samples were selected, and the normal metal bridge was further patterned by ion milling to increase the junction resistance. We found that extreme care

was required to avoid electrostatic damage to the chips when the junction resistances exceeded 1 Ω. Fig. 2 (b) shows an optical micrograph of the feed area of a completed device.

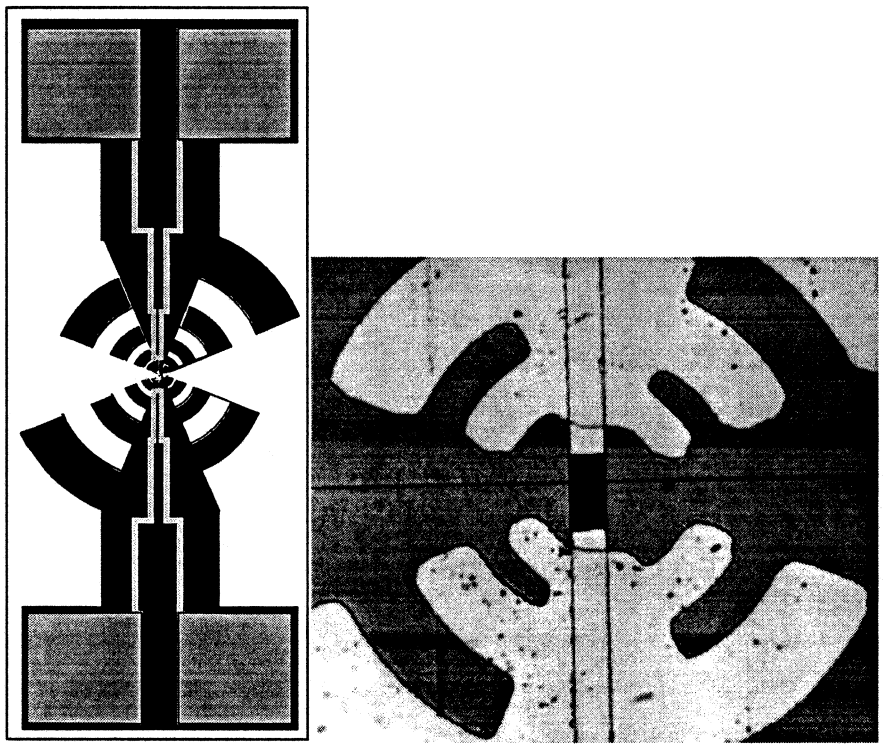

Fig. 2 (a) Schematic of normal metal planar log periodic antenna (black) and YBCO contact pad and lead (grey) configuration for the chips used in the far infrared measurements. (b) An optical micrograph of the feed area and part of an antenna from an actual chip. The junction width is 6 μm. The dark area at the feed is the YBCO exposed by the angled ion mill.

III. Measurement Apparatus

The experimental configuration is shown in Fig. 3. The samples were mounted in vacuum, on a variable temperature stage, with a 1 cm radius high resistivity Si hemisphere pressed against the backside of the substrates. A 6.5 THz cutoff lowpass filter, cooled to 4 K, was used to reduce the thermal infrared (IR) background to a manageable level. Nonetheless, residual IR power absorbed on the sample stage was sufficient to raise its temperature approximately 5 K above the liquid He bath, limiting our measurements to $T > 9$ K. The broadband IR power coupled directly into the junction

via the antenna may be estimated as P_{bg} = kTB = 30 nW, with T = 300 K and the bandwidth B limited by the filter cutoff. Plano convex lenses machined from high and low density polyethelyne were used to focus the far infrared laser into the dewar. The focussing was relatively slow, with a maximum opening angle of ~10° (FWHM), which resulted in a large loss (roughly 16 dB) due to beam mismatch with the antenna. The far-IR laser, pumped by a 15 W CO_2 laser, yielded approximately 5 mW on the formic acid lines at 404, 760, and 992 GHz, and approximately 8 mW on the 2.52 THz methanol line. A substantial fraction of the laser power was directed by a (Si or mylar) beamsplitter into a pyroelectric detector to serve as a real time power monitor. Based on these rough estimates of coupling efficiencies, the maximum laser power actually delivered to the junction was in the range of 50 μW. The laser power was adjusted by varying the gas pressure. The junctions were biased through a 1 kΩ resistor. Voltages and currents were amplified by low noise instrumentation amplifiers and current voltage characteristics (IVCs) were plotted on either an xy recorder or an oscilloscope.

IV. Results

We measured two junctions with the far infrared laser. The first initially had a resistance of 16 Ω and a critical current of 0.43 mA at 4.2 K. Shortly after the far-IR measurements were begun, during a brief hiatus in the experiments, the resistance increased to 38 Ω and the critical current dropped to 0.28 mA. This change was possibly due to degradation of some portions of the junction due to prolonged contact with a vaccuum environment at room temperature. We also measured a second junction with a resistance of 12 Ω and a critical current of 0.22 mA. We have fabricated other junctions of this type, but without antennas, for studies of the temperature dependence of the critical currents. Fig. 4 shows a plot of the temperature dependence of I_CR_N and R_N for a typical high I_CR_N junction. Fig. 5 shows the current-voltage curves for the 10 mV I_CR_N junction with no applied radiation, and with radiation at 404 GHz, 760 GHz, and 992 GHz. The Shapiro steps are clearly visible with minimal rounding, and extend to high voltages, approximately 15 mV (corresponding to 7 THz) at a temperature of 9 K, and approximately 6 mV (3 THz) at a temperature of 53 K. It is also obvious that the current voltage characteristic is mildly hysteretic with no rf bias applied. Fig. 6 shows measured current-voltage characteristics at 53 K with and without 992 GHz laser radiation applied.

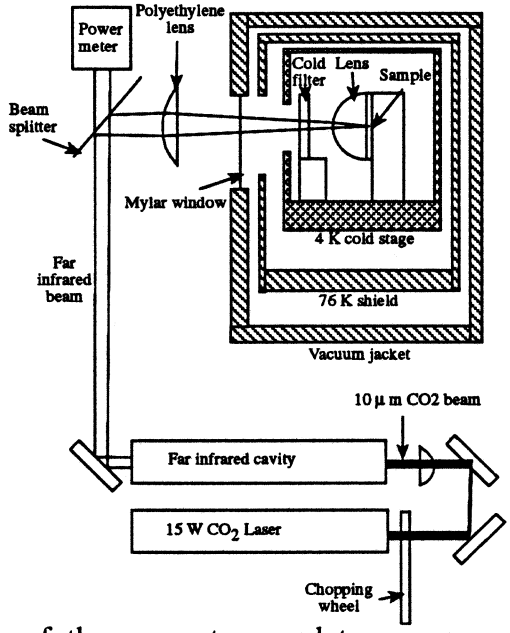

Fig. 3 Schematic of the apparatus used to measure shapiro Steps at THz Frequencies.

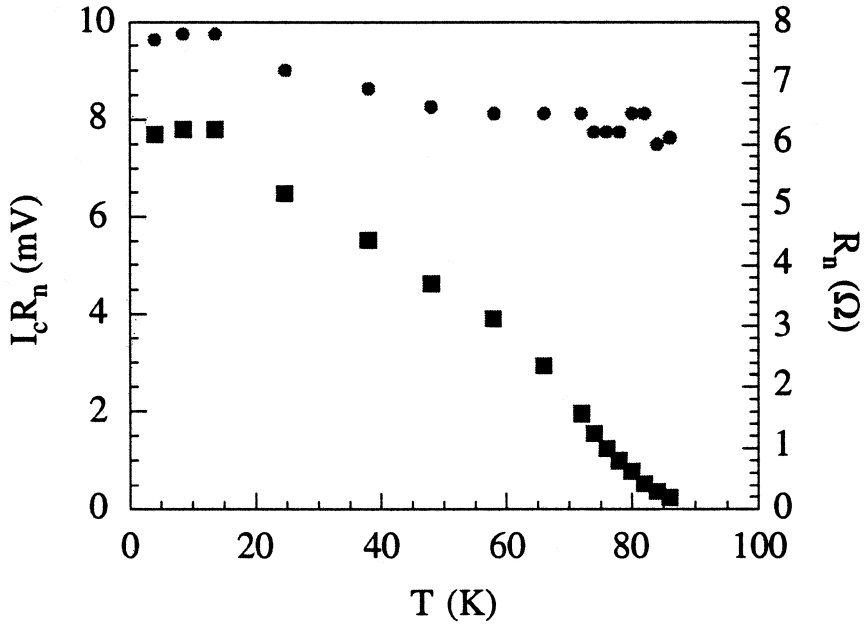

Fig. 4 Temperature dependence of the normal state resistance R_N and the I_cR_N product of a typical high resistance junction. The squares represent values of the I_cR_N product and the circles represent the normal state resistance.

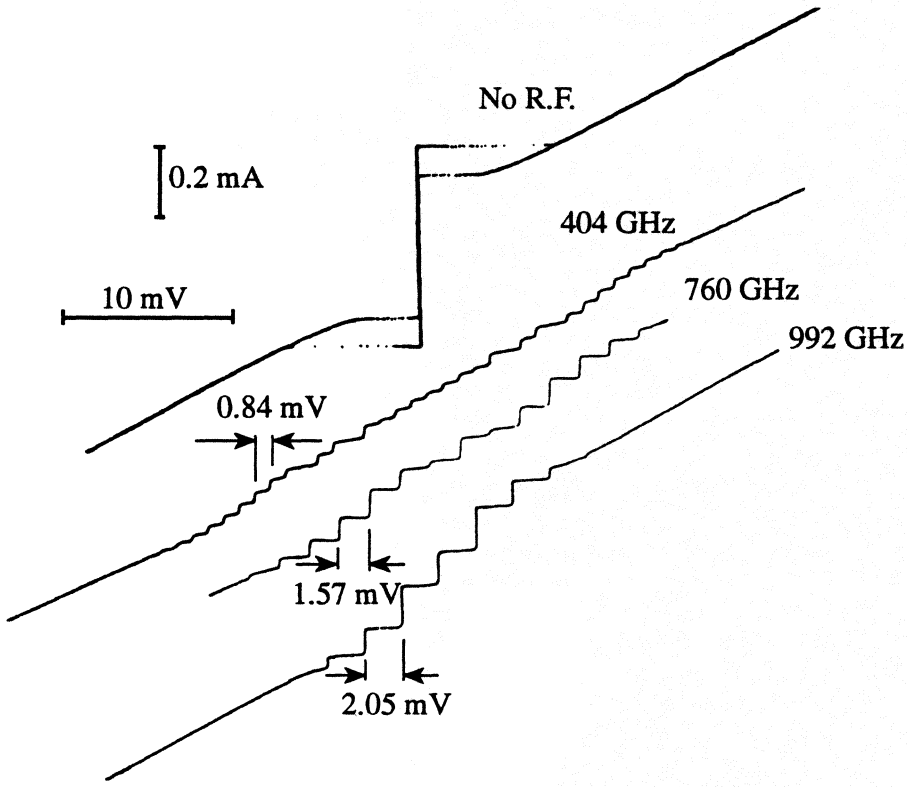

Fig. 5 dc Current Voltage characteristic taken at 9 K of a junction with a resistance of 38 Ω and a critical current of 0.28 mA. IV Curves are also shown for applied R.F. frequencies of 404 GHz (Ω = .08), 760 GHz (Ω = 0.15), and 992 GHz (Ω = 0.19) showing pronounced Shapiro steps at voltages comparable to the 10 mV I_CR_N product.

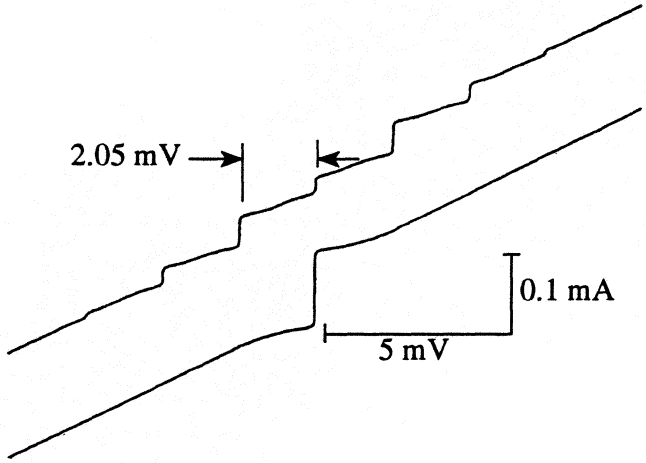

Fig. 6 Current voltage characteristics at 53 K. The upper curve shows the current voltage characteristic with 992 GHz (Ω = 1.1) radiation.

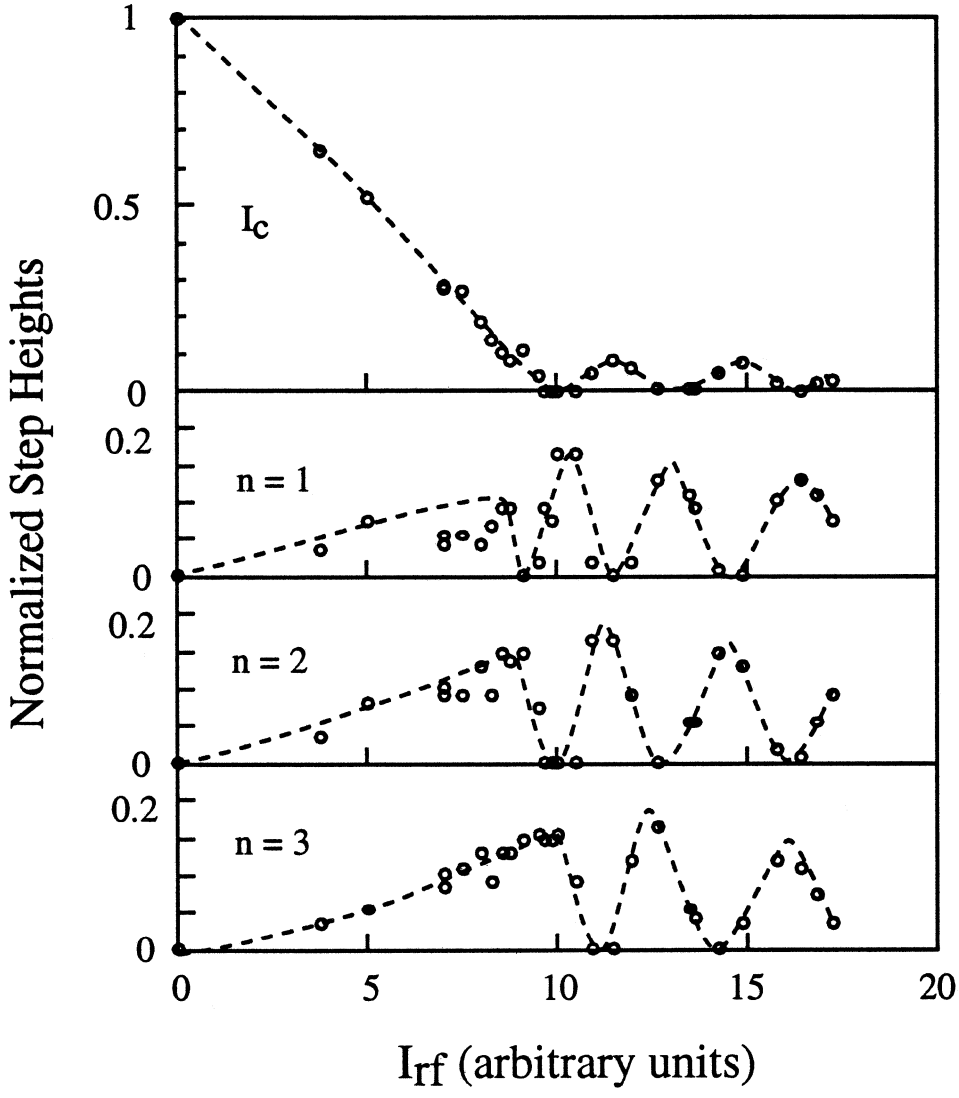

Fig. 7 Power dependence of the critical current and Shapiro step heights for a 10 mV I_CR_N junction at 9 K irradiated at 404 GHz. For the measured values of I_C and R_N of 0.28 mA and 38 Ω this corresponds to a reduced frequency Ω= 0.08. The critical current and step heights are normalized to the value of the critical current with no rf applied. The R.F. current quoted in arbitrary units was assumed proportional to the square root of the measured power. The dashed lines through the points are guides to the eye.

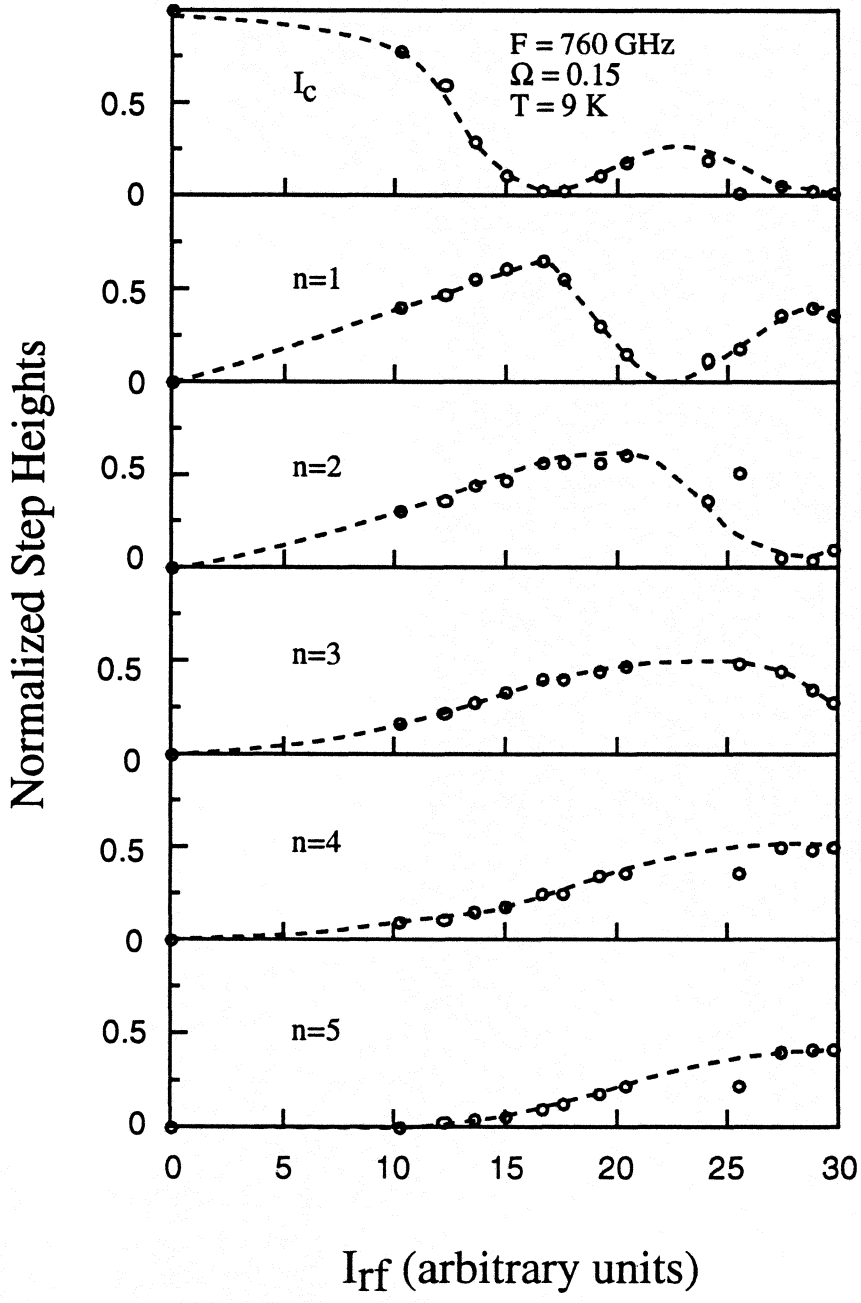

Fig. 8 Power dependence of the critical current and Shapiro step heights for a 10 mV I_CR_N junction at 9 K irradiated at 760 GHz. For the measured values of I_C and R_N of 0.28 mA and 38 Ω this corresponds to a reduced frequency Ω= 0.15. The critical current and step heights are normalized to the unirradiated critical current. The rf current quoted in arbitrary units was assumed proportional to the square root of the measured power. The lines through the points are meant as guides to the eye.

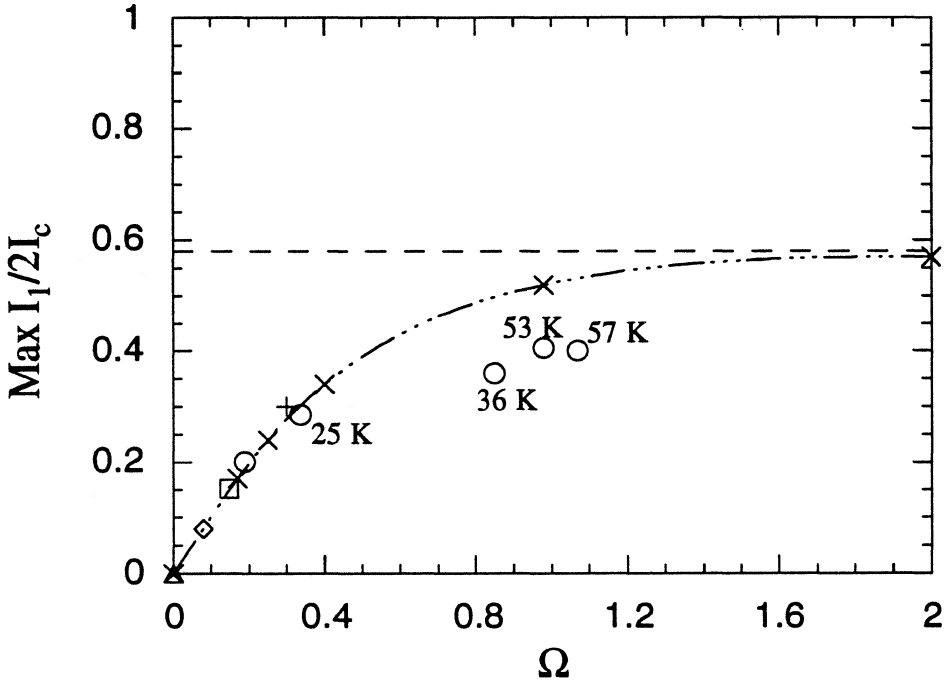

Fig. 9 Dependence of maximum normalized amplitude of first Shapiro step vs reduced frequency Ω. The circles, the square, diamond and triangle refer to data taken at 992 GHz, 760 GHz, 404 GHz and 3 GHz, respectively. The cross refers to data taken from a second device with a 3 mV I_cR_n product at 992 GHz. Points without explicitly labeled temperatures were taken at 9 K. The dashed line is the Bessel function value obtained for large β_c. The dot dashed curve and the X's are the results of simulations of the zero temperature (overdamped)RSJ model from Kautz et al[8] and from Benz.[12] Here β_c, the Stewart-McCumber parameter, is given by $\beta_c = 2\pi$ (2e/h) $I_cR_N^2C$ where e is the electron charge, h is Planck's constant and C is the shunt capacitance.

In Figs. 7 and 8 we show the measured power dependence of the Shapiro step heights as a function of the applied power. The characteristic pattern of lobes is qualitatively similar to what would be expected from the resistively shunted junction model. The frequency dependence of the step amplitudes is a feature that can be checked against various models. This allows a direct comparison with the predictions of the R.S.J. model (or other dynamical models) without explicitly knowing the R.F. power levels. In Fig. 9 we show the maximum amplitude of the first Shapiro step normalized to twice the critical

current, from two devices, as a function of reduced frequency $\Omega = hF/2eI_cR_N$. The data shown in Fig. 9 were taken using 3 GHz, 404 GHz, 760 GHz and 990 GHz radiation over a range of temperatures so as to access a wide range of reduced frequencies. One can see that there is a systematic variation, approximately linear at low frequencies, with a slope close to 1.0, rolling off as Ω approaches unity. For comparison, some points calculated at low reduced frequency using the overdamped ($\beta_C = 0$) RSJ model are also shown in Fig. 9. From this we can see that the agreement with the RSJ model is excellent at low frequencies. At frequencies near unity the maximum step height is still somewhat lower than the high frequency Bessel function prediction ($I_1/I_C = 0.58$) of the RSJ model. Considering the uncertainties due to the frequency dependence of the embedding impedance, it is unclear to what extent the data should agree quantitatively with the RSJ model at high reduced frequencies. A further uncertainty arises because the frequency dependence of the supercurrent is unknown for frequencies comparable to the gap frequency, whereas the RSJ model assumes a frequency-independent supercurrent. These effects are all progressively more important at higher frequencies, which is exactly the region where the observed deviations from the RSJ model are most pronounced.

An correlation was observed between the junctions' characteristic voltages and the maximum observable Shapiro step frequency. For the two junctions measured we found strong Shapiro steps only up to frequencies comparable to the junction's characteristic frequency. The junction with the 10 mV characteristic voltage showed Shapiro steps up to approximately 15 mV, while the junction with the 3.0 mV characteristic voltage showed Shapiro steps only up to 4 mV with a 404 GHz source. The 3 mV junction showed only one step when biased with a 990 GHz beam. The observed proportionality of scale between the highest voltage Shapiro steps and the I_CR_N product suggests that the difference in the I_CR_N product for the two junctions measured is related to a difference in the intrinsic Josephson coupling strength. We speculate that the observed behavior is due to a combination of differing normal metal bridge length, S-N interface boundary resistance, or reduced energy gaps in the superconducting banks.[13] Junctions with identical Josephson coupling strength but differing parasitic shunt conductance would be expected to exhibit Shapiro steps out to similar maximum voltages (but with power dependence characteristic of different reduced frequencies) which we have not observed. To the extent that this observed behavior will prove to hold generally for this class of junctions we suggest that optimal high frequency locking will be achieved with junctions with the highest possible characteristic voltages. The junctions reported here have

already exhibited Shapiro steps at voltages as high as the best point contact junction results, and higher than any other high T_c technology.

The 10 mV junction exhibited no Shapiro steps when illuminated with 2.52 THz radiation. This result for the 10 mV junction is most likely not intrinsic to the junction dynamics, but rather, it is due to a combination of two extrinsic effects: the opacity of the LaO_3 substrate, which rises substantially above 1 THz, and the high frequency cutoff of the antenna. The 2.52 THz tranmissivity of an LaO substrate was separately measured to be 0.12, while reflection loss (with $\varepsilon_r = 24$) would only account for a loss of approximately 50 %.

Hysteresis in junction current voltage characteristics is most commonly due to either underdamped dynamics[14,15] or to self-heating.[16] A thermal explanation for the observed hysteresis requires invoking thermal conductances that are implausibly small. The bias heating in the junction is of the scale $I_c^2R_N$, which is 3 μW for a junction with a resistance of 38 Ω and a critical current of 0.28 mA. The observed 30% hysteresis at 9 K would require bias heating of at least 15 K. This would imply a thermal conductance between the junction and the substrate of $.2*10^{-7}$ W/K, which is about two orders of magnitude smaller than is typically obtained in structures of this size. In our junctions, there is significant evidence that the hysteresis is primarily due to underdamped dynamics, i.e. the Stewart-McCumber parameter $\beta_c = 2\pi$ (2e/h) $I_cR_N^2C \geq 1$, where e is the electron charge, h is Plancks constant, C is the shunt capacitance and I_c and R_N are the critica current and normal resistance. Using dynamical simulations within the context of the resistively shunted junction model one can calculate the β_c of a junction from its critical current, and its return or retrapping critical current.[17] We performed this procedure for the 10 mV junction. We measured the retrapping critical current over a range of temperatures (and therefore critical currents), and extracted a value for β_c, giving us the capacitance at each temperature. For these calculations we replaced the normal state resistance of the junction with the parallel combination of the estimated antenna impedance and the measured junction resistance R_N. This assumption is justified because the voltages at which the junction retrapped were all within the nominal bandwidth of the antenna, and in this way we better include the additional damping of the junction due to the antenna radiation resistance. From the simulations, we calculated a value of ~4.5 fF for the capacitance . Fig. 10 shows the capacitance extracted from the retrapping currents over a range of critical currents taken at various temperatures.

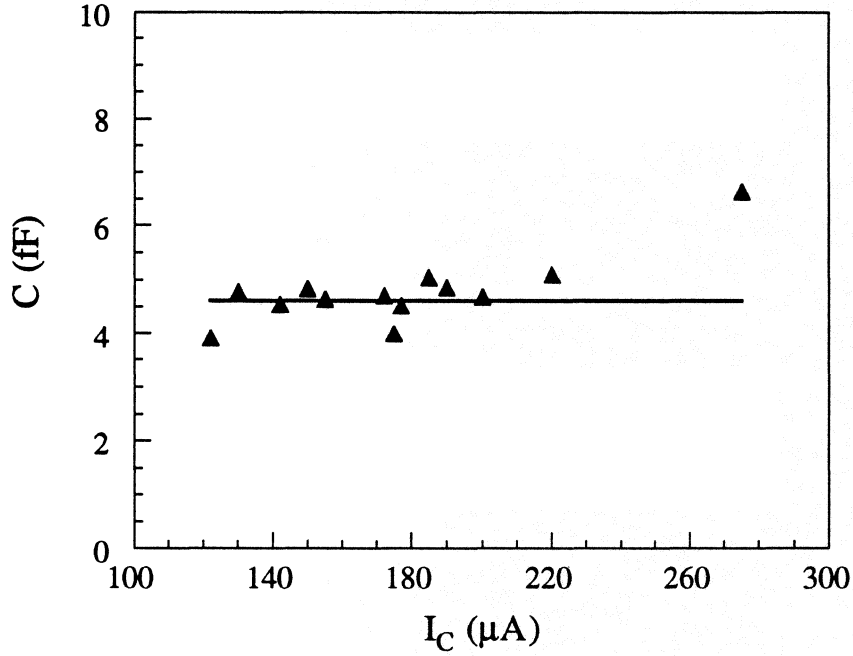

Fig. 10 Values of capacitance extracted from the retrapping and critical currents of a 10 mV IcRn Junction. Each point was taken at a different temperature, which ranged from 9 K to 45 K.

The value of the capacitance calculated in this way is within a factor of 2 of our estimate of the geometric capacitance of the electrodes within the feed of the antenna. The remarkable consistency of the capacitance over a wide temperature range (9 K to 50 K) is strong evidence that the hysteresis is due primarily to dynamical effects and that self heating is at most a second order effect. We have observed similar behavior in the other junctions that displayed hysteresis. In addition, over the regime where the current voltage characteristics were hysteretic, we observed that at sufficiently high applied far-IR power the adjacent Shapiro steps were overlapping in current. i.e.. the steps themselves were mildly hysteretic. This behavior was not observed when the D.C. I-V curves were nonhysteretic. Within the contexct of the RSJ model, such behaviour only occurs for underdamped dynamics where $\beta_C \geq 0.7024$. It is unlikely that self heating would lead to a consistent value of RSJ derived capacitance over such a wide temperature range.

To summarize, we have fabricated high temperature superconducting Josephson junctions with I_CR_N products up to 10 mV. Measurements of the Shapiro steps induced by a far infrared laser showed RSJ-like behavior with visible steps at Josephson frequencies up to 8 THz. The high resistances of this type of junction make them attractive candidates for use in antenna based quasioptical coupling schemes. The wide operating temperature range and fast non-thermal (i.e. Josephson) response mechanism gives these devices an intrinsic flexibility well suited to many applications in THz detection and mixing.

---

[1]P. L. Richards, "Semiconductors and Semimetals," V c1.12, (Academic Press, New York 1977) Chapter 6

[2] R.J. Schoelkopf, T.G. Phillips, and J. Zmuidzinas, IEEE Trans. Appl. Superconductivity, in press (1993)

[3]K.K. Likharev, Rev. Mod. Phys.,**51** (1) 1979

[4]D. Dimos, P. Chaudhari, J. Manhart, and F. K. LeGoues, Phys. Rev. Lett, **61**, 219, (1988)

[5]K. Char, M. S. Colclough, S. M. Garrison, N. Newman, and G. Zaharchuck, Appl. Phys. Lett., **59**,733, (1991)

[6]M.S.DiIorio, S. Yoshizumi, K. Y. Yang, J. Zhang, and M. Maung, Appl. Phys. Lett., **58**, 2552, (1991)

[7]R. H. Ono, J. A. Beall,, M. W. Cromar, T. E. Harvey, M. E. Johansson, C. D. Reintsema, and D. A. Rudman, Appl. Phys. Lett., **59**, 1126, (1991)

[8]R. L. Kautz, R. H. Ono, and C. D. Reintsema, Appl. Phys. Lett. **61** (3), p. 342 (1992)

[9]N. Missert, C. D. Reintsema, J. A. Beall, T. E. Harvey, R. H. Ono, and E. A. Rudman, to be published in I.E.E.E. Trans. Applied Supercond. in the proceedings of the Applied Superconductivity Conference 1992

[10]R. H. DuHamel and D. E. Isbell, Broadband Logarithmically periodic antenna structures," *IRE Nat. Conven. Rec.*, pt. 1, 1957, pp. 119-128

[11]D. B. Rutledge, D. P. Keikirk, and D. P. Kasilingam, "Integrated Circuit Antennas," *Infrared and Millimeter Waves, Vol. 10*, (Academic Press, N.Y. 1983), p. 1.

[12]S. P. Benz private communication

[13]M. Y. Kupriyanov and K. K. Likharev, Sov. Phys. Usp. **33**,(5) May 1990

[14]W. C. Stewart, Appl. Phys. Lett., **12**, 277 (1968)

[15]D. E. McCumber, J. Appl. Phys., **39**, 3113 (1968)

[16]W.J.Skocpol, M.R.Beasley, and M.Tinkham, J. Appl. Phys., **45**, 4054 (1974)

[17] A. Barone and G. Paterno "Physics and Applications of the Josephson Effect,"John Wiley and Sons, Inc (1982)